High-frequency giant magnetoresistance measurement to study the dynamics of a micron-scale spin-valve sensor

N. Biziere[1,2] and C. Fermon[2]

[1]*Institut de Physique des Nanostructures, Ecole Polytechnique Fédérale de Lausanne (EPFL), EPFL-SB-IPN Station 3, 1015 Lausanne, Switzerland*

[2]*DSM/IRAMIS/Service de Physique de l'Etat Condensé (SPEC), CNRS URA 2464, CEA Saclay, 91191 Gif-sur-Yvette Cedex, France*

(Received 13 February 2008; revised manuscript received 4 July 2008; published 12 August 2008)

We report on the study of the magnetization dynamic of a single micrometric spin-valve element by high-frequency giant magnetoresistance measurement. We have combined transport measurements in the microwave range and large band ferromagnetic resonance with microantennas. The spin valve is used as an *in situ* demodulator to probe the individual dynamics of each layer and the relative phase of their oscillations. We deduce the conditions for coupling the hard and free layer dynamics and show the influence of a static magnetic configuration on the sensitivity of spin valves in the microwave range. This work offers a different approach for studying the dynamics of single isolated micron-sized systems.

DOI: 10.1103/PhysRevB.78.064408 PACS number(s): 76.50.+g, 72.25.−b, 73.43.Fj

Dynamics of small magnetic multilayer elements are extensively studied for their use in read heads[1–3] and their potential applications as microwave sources.[4–6]

In particular, spin-valve structures are now extensively used for magnetic read heads in storage devices. In this field the constant decrease in size of magnetic bits and the increase in speed of the electronics lead read heads to work at frequencies in the gigahertz range. As a consequence the understanding of the magnetization dynamics of spin valves has become a key point for the future of storage application.

In exchange biased spin valves, most attention has been paid to the free layer dynamics as shown for example in spin-torque experiments.[7–9] However, the complex structure made of several magnetic layers with different magnetic properties and the possibility of coupling between layers refine the dynamics mechanisms. In this paper we show that both the free and hard layers are involved in the process and experimental evidence for dynamic coupling is given.

The spin valve is used as an *in situ* demodulator and the giant magnetoresistance (GMR) is used as a probe of the magnetization dynamics. A microwave magnetic field is supplied to a micron-sized spin-valve sensor by a microantenna. This excites and measures the dynamics of the system. At the same time, an oscillating voltage whose frequency is different from the magnetic excitation is applied to the sensor in the current-in-plane configuration. As the GMR effect is the only nonlinear process in the system, we obtain an electrical response at a demodulated frequency directly proportional to ΔR (the difference of resistance in ohms between the parallel and antiparallel magnetic state) and to the susceptibilities of the different layers. This technique avoids any interference that could appear in the microwave measurements. For example, we have shown[10] that the current induced by the magnetic excitation is the source of an increase in the dc voltage of the sensor.

The spin-valve stack $Ta/NiFe_{(3.5\ nm)}/CoFe_{(1.2\ nm)}/Cu_{(2.9\ nm)}/CoFe_{(2.5\ nm)}/Ru_{(0.7\ nm)}/CoFe_{(2\ nm)}/IrMn_{(10\ nm)}/Ta$ is sputtered onto a thick glass substrate in high-vacuum atmosphere. The first NiFe/CoFe bilayer corresponds to the free layer of the sensor and acts as a single magnetic layer presenting a growth induced uniaxial anisotropy field H_k of 5 Oe. The second and third CoFe layers correspond to the hard and quenched layers, respectively, and are antiferromagnetically coupled by Ruderman-Kittel-Kasuya-Yoshida (RKKY) interaction. The free and hard layers are those of interest for the GMR effect since most of the current flows in the copper layer. We assume the quenched layer magnetization to be independent of the external magnetic field because of the strong interfacial coupling with the IrMn.

Orange peel coupling favors a parallel alignment of the hard and free layer magnetizations at zero field. dc GMR measurements give a value of 12 Oe for the corresponding bias field H_{bias} acting on the free layer.

The sensor is designed in a yoke shape (Fig. 1) by conventional UV lithography techniques combined with ion milling in an argon atmosphere. The longest part of the sensor is aligned in the easy axis direction ensuring uniform magnetizations.

Slotline waveguides are deposited on the sensor by lift off of $Ti_{(10\ nm)}/Cu_{(200\ nm)}/Au_{(10\ nm)}$ for broadband (dc to 20 GHz) electrical measurements. The amplitude of the current flowing in the sensor is calibrated by measuring the complex impedance of the system slotlines/sensor with a network analyzer.

The microantenna (Fig. 1) is deposited by lift off of $Ti_{(10\ nm)}/Cu_{(200\ nm)}/Au_{(10\ nm)}$ on top of the sensor after deposition of a 300-nm-thick Si_3N_4 insulating layer. The central conductor is aligned with the long bar of the sensor with a precision of 0.5 μm. The amplitude of the pumping field h_0 created by the antenna is determined from its electrical parameters and $h_0=I/2w$ where I is the amplitude of the current in the central conductor and w is the width of the central conductor. At low frequencies vector network analyzer measurements have shown that the antenna can be well modeled as a resistor-inductor circuit.

The magnetization dynamics is first studied by ferromagnetic resonance (FMR) with the microantenna. The experiment is performed with $\Theta_1=\Theta_2=\Theta_3=0$. The sensor dynamic susceptibility is extracted from the antenna reflected

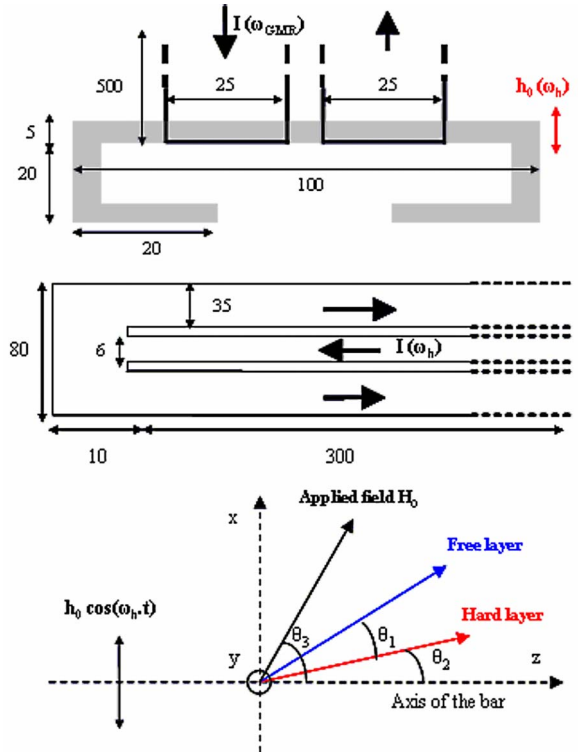

FIG. 1. (Color online) (Top) Dimensions of the sensor designed as a yoke shape (gray) and the contact pads (delimited by black lines). (Middle) Dimensions of the shorted antenna. All dimensions are given in μm. (Bottom) System of axis and relative orientation of the different magnetic quantities.

input voltage since it induces a change of the antenna self-inductance.[11,12] We deduce that the resonance pulsation ω_r dependence on the external field H_0 follows the Kittel uniform resonance mode[13] of an infinite rectangular thin plate (Fig. 2) as we could expect from the symmetry of the pumping field. ω_r can be written as

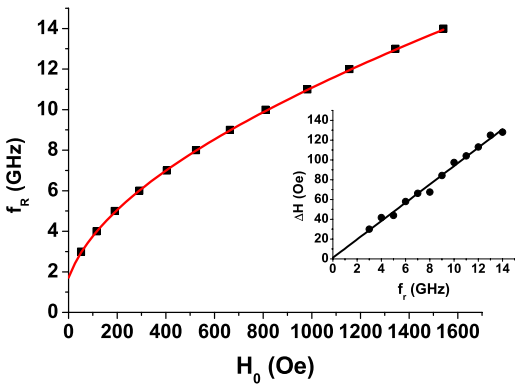

FIG. 2. (Color online) Resonance frequency of the spin valve as a function of H_0 (black squares) and fit obtained with Eq. (1) (red line). The parameters of the fit are given in the text. The inset presents the ferromagnetic linewidth as a function of the resonance frequency (black circles) and linear fit (black line) $\Delta H = \alpha\omega_r / \gamma\mu_0$ with $\alpha = 0.026$.

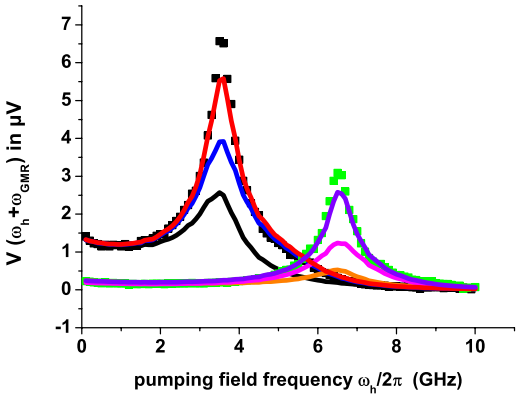

FIG. 3. (Color online) Demodulated signal as a function of the pumping field frequency measured with a spectrum analyzer in the parallel magnetic orientation of the free and hard layer at 100 (black square) and 320 Oe (green square). The black and orange lines correspond to the fit with Eq. (4) for 100 and 320 Oe, respectively. The blue and magenta lines correspond to the fit with Eq. (5) for 100 and 320 Oe, respectively. The red and violet lines correspond to the fit with Eq. (5) including the dynamic dipolar coupling.

$$\omega_r = \gamma\mu_0 \sqrt{[H_0 + H_k + H_{\text{bias}} + (N_x - N_z)M_s]} \times \sqrt{[H_0 + H_k + H_{\text{bias}} + (N_y - N_z)M_s]}, \quad (1)$$

where $(\gamma/2\pi) = 29$ GHz/T is the gyromagnetic factor, M_S is the magnetization at saturation, and N_x, N_y, and N_z are the demagnetizing factors. The best fit has been obtained for values $N_x = 1.110^{-3}$, $N_y = 1 - N_x$, and N_z assumed equal to zero—reflecting the aspect ratio of the sensor and the approximation of an infinite thin film. The magnetization at saturation obtained is $\mu_0 M_S = 1.3$ T. This result is in good agreement with the value of 1.2 T obtained by superconducting quantum interference device and FMR measurements on a reference continuous NiFe/CoFe film deposited in the same conditions.

The dependence of the FMR linewidth as a function of the applied field (inset in Fig. 2) gives a value of the Gilbert-type damping coefficient $\alpha = 0.026$. The same coefficient value has been measured on the reference NiFe/CoFe film and is in good agreement with literature values for damping coefficients in ultrathin films.[14–16]

The magnetization dynamics is then studied by *in situ* demodulated electrical measurement. The signal is obtained by applying an oscillating voltage to the sensor. In the presence of the magnetic excitation, the time dependence of the voltage is written as

$$V(t) = \left(R_0 + \Delta R \frac{\vec{M}_{FL} \cdot \vec{M}_{HL}}{2\|\vec{M}_{FL}\| \cdot \|\vec{M}_{HL}\|} \right) \times [I_{\text{GMR}} \cos(\omega_{\text{GMR}} t + \varphi_{\text{GMR}}) + I_{rf} \cos(\omega_h t + \varphi_h)] + V_{rf}(\omega_h), \quad (2)$$

where R_0 is the average resistance of the sensor and $\vec{M}_{FL}$ and $\vec{M}_{HL}$ are the free and hard layer magnetization vectors,

respectively. I_{GMR}, ω_{GMR}, and φ_{GMR} and I_{rf}, ω_h, and φ_h are the amplitude, pulsation, and phase of the current injected and the current, pulsation, and phase induced by the microwave magnetic field in the sensor, respectively. V_{rf} is a voltage induced in the slotlines by the inductive coupling with the microantenna.

The GMR effect presents the same time dependence as the magnetic excitation because of the dynamic susceptibility of the sensor. When we develop Eq. (2), with $\Theta 1 = \Theta 3$ and $\Theta 2 = 0$ (keeping only the terms linearly dependent on ω_h and ω_{GMR}), we obtain a contribution from the GMR effect of the form

$$V(t) = \Delta R\, I_{GMR} \cos(\omega_{GMR} t + \varphi_{GMR}) \left\{ \frac{\cos \Theta_1}{2} \left[1 - \frac{\chi_{FL}^2 h_0^2 \cos^2 \Theta_1}{4M_{SF}^2} - \frac{\chi_{FL}^2 h_0^2 \cos^2 \Theta_1 \cos(2\omega_h t)}{4M_{SF}^2} \right] + \frac{\sin \Theta_1 \chi_{FL} h_0 \cos \Theta_1 \cos(\omega_h t)}{2M_{SF}} \right\}, \tag{3}$$

where χ_{FL} is the free layer complex susceptibility deduced from the FMR measurements. Here we assume that the hard layer does not experience the magnetic excitation since the RKKY interaction with the quenched layer can be modeled as a high effective field.

When Θ_1 is different from zero, the product of the different cosines gives two series of signals at frequencies $[\omega_h + (-\omega_{GMR})]/2\pi$ and $[2\omega_h + (-\omega_{GMR})]/2\pi$ directly proportional to ΔR ($-1,4$ ohms for our sample) and χ.

We present in Fig. 3 the demodulated signal at the frequency $[\omega_h + (-\omega_{GMR})]/2\pi$ for $\Theta_1 \approx \pi/10$ measured with a spectrum analyzer. Following Eq. (3), the signal is nominally,

$$V_{GMR}(\omega_h \pm \omega_{GMR}) = \frac{|\sin \Theta_1|\, |\cos \Theta_1|\, |\Delta R|\, \|I_{GMR}(\omega_{GMR})\|\, \|h_0(\omega_h)\|\, \|\chi(\omega_h)\|}{4M_{SF}}. \tag{4}$$

Equation (4) describes the profile of the experimental signal but does not fit with the amplitude, especially around the resonance (black and orange lines in Fig. 3). This mismatch is better represented by the ratio of the experimental signal over the simulated signal (Fig. 4). This quantity reflects the difference between the susceptibility of the free layer and the "true" susceptibility of the sensor, or in other words, the difference between the simulation and the experiment for the dynamic angle Θ_1.

This ratio is frequency dependent. We observe two peaks for low fields (100 Oe) and only one peak at higher field (320 Oe). We explain this feature assuming a small oscillation of the hard layer and the relative phase between the free and the hard layer precession.

We first make the assumption that the hard layer resonance occurs at a higher frequency than the free layer. This implies that the first and second peaks observed at $H_0 = 100$ Oe correspond to the resonance of the free and hard layers, respectively. At low frequencies, both layers oscillate in phase with the magnetic excitation. When the free layer resonance is reached, the two layers oscillate in an out-of-phase configuration with respect to h_0. As both magnetizations are pushed back from each other, it leads to a more important dynamic angle Θ_1 than expected for a single layer precession and so an increase in the experimental signal. Then, when the hard layer resonance is excited, Θ_1 increases until both layers get back in phase.

When introducing the hard layer dynamics in our calculation and keeping only the terms linear with ω_h, we get a contribution from the GMR effect such as

$$\frac{\vec{M}_{FL} \cdot \vec{M}_{HL}}{2\|\vec{M}_{FL}\| \cdot \|\vec{M}_{HL}\|} = \left[\frac{\chi_{HL}(\omega_h)\cos(\Theta_2)}{M_{SH}} - \frac{\chi_{FL}(\omega_h)\cos(\Theta_3)}{M_{SF}} \right] \frac{\sin(\Theta_1) h_0 \cos(\omega_h t)}{2}, \tag{5}$$

where χ_{HL} is the hard layer dynamic susceptibility. Calculations are performed assuming a uniform precession of the hard layer and χ_{FL} is the same as used to solve Eq. (4). The hard layer resonance frequency is supposed to follow the Kittel mode described by Eq. (1).

The result of this model (blue and magenta lines on Fig. 3) gives a flatter ratio as shown in Fig. 4, which tends to validate a uniform precession in a large frequency range. It allows to deduce the parameters of the hard magnetic layer.

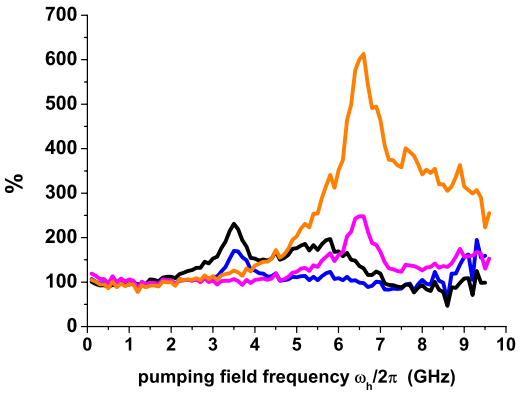

FIG. 4. (Color online) Ratio of the experimental over the simulated signal as a function of the pumping field frequency for 100 Oe (black), 320 Oe (orange), and the two layers precession model at 100 (blue) and 320 Oe (magenta) without including the dipolar coupling.

The best fit has been obtained for $\mu_0 M_S = 1.3$ T, an effective bias field acting on the CoFe of 200 Oe and a damping parameter $\alpha_{HL} \approx 0.07$. We assume the high value of α_{HL} to be ascribed to the magnon relaxation at the different interfaces and to the coupling between the hard and quenched layers.

In spite of the good agreement over a large frequency range between the two-susceptibility model and the experimental data, we still observe a discrepancy around the free layer resonance. This effect is emphasized at high fields for which the free and hard layer resonance frequencies approach each other (6.6 and 7.5 GHz for the free and hard layers, respectively, at $H_0 = 320$ Oe). In this case, both layers seem to act as if they were coupled similarly to optical modes (π-radian out-of-phase oscillation) observed in magnetic multilayers.[17,18] This result clearly shows that the magnetization dynamics in the spin valve can be well described by the precessions of isolated layers in the nonresonant regime but that some interaction has to be encountered in the resonant regime.

To explain this effect one must find a mechanism coherent with the two-susceptibility model presented above, but that induces an increase in Θ_1 around the resonance. The peak frequencies on Fig. 4 lead us to believe that the free layer dynamics drives the hard layer magnetization. Then we propose that the appearance of the dynamic coupling is linked to the dynamics of the free layer. This effect is taken into account in our model described by Eq. (5) by assuming that the dynamic field acting on the hard layer is the sum of h_0 and a dynamic dipolar field of the form $-\mathbf{m_{FL}}N$, where $\mathbf{m_{FL}} = \chi_{FL} h_0$ represents the dynamic part of the free layer magnetization. Then if the dynamic dipolar field is bigger than h_0, then the phase of the hard layer dynamics as compared to h_0 will be opposite to the free layer's one. The results are presented in Fig. 3 by the blue and violet lines for a coefficient $N = 0.001$. This coefficient gives an amplitude of the dipolar field of about 9 Oe at the free layer resonance for $H_0 = 370$ Oe (and $h_0 \sim 3$ Oe at resonance). Even if the matching is not perfect, the agreement with the experimental data is excellent and tends to validate this approach. Let us note that its amplitude is the order of magnitude as H_{bias}. This could mean that the physical origin of the effective demagnetizing factor is linked to the orange peel coupling. This would imply that technological process has an importance on the dynamics of the system.

In this paper transport measurements have been performed on a micron-sized spin-valve sensor used as an *in situ* demodulator. We have applied to a micron scale some techniques used in the fields of FMR and high-frequency electrical measurements.

We have shown that the GMR effect offers a very attractive option to measure the dynamics of magnetic multilayers since it gives information about the relative phase of the precession of each individual layer. Moreover it offers a different approach for studying the magnetization dynamics of micron and submicron devices. One particular interest compared to inductive measurements is that the electrical signal is not proportional to the magnetic volume and so it can be applied to a single system, avoiding all the problems related to arrays of elements.

One major result of this work concerns the future of read heads application. Indeed, we show that the sensitivity of the sensor in the microwave regime depends also on the hard layer dynamics. Moreover, we show that the dynamics of the sensor cannot be simply described by the dynamics of isolated layers but dynamic dipolar coupling must be taken into account. By consequence this raises the question of the future technology that should be applied for read heads working in the microwave range. It becomes obvious that the susceptibilities of all magnetic layers must be used to increase the sensor sensitivity. In this case the use of a hard layer is no more relevant but coupled magnetic layers with low-coercive fields must be considered.

The authors would like to thank the "Magnetism and Spintronics" group from the Trinity College of Dublin (Ireland) for providing spin-valve films and M. Viret for fruitful discussions. This work was supported by RTN network dynamics and the project Biomagsens under Grant No. NMP4-CT-2005-07210.

[1] P. P. Freitas, F. Silva, N. J. Oliveira, L. V. Melo, L. Costa, and N. Almeida, Sens. Actuators, A **81**, 2 (2000).

[2] H. Kanai, K. Yamada, K. Aoshima, Y. Ohtsuka, J. Kane, M. Kanamine, J. Toda, and Y. Mizoshita, IEEE Trans. Magn. **32**, 3368 (1996).

[3] M. Takagishi, K. Koi, and M. Yoshikawa, IEEE Trans. Magn. **38**, 2277 (2002).

[4] W. H. Rippard, M. R. Pufall, S. Kaka, S. E. Russek, and T. J. Silva, Phys. Rev. Lett. **92**, 027201 (2004).

[5] T. Devolder, A. Meftah, K. Ito, J. A. Katine, P. Crozat, and C.

Chappert, J. Appl. Phys. **101**, 063916 (2007).
[6] F. B. Mancoff, N. D. Rizzo, B. N. Engel, and S. Tehrani, Nature (London) **437**, 393 (2005).
[7] F. Wegelin, D. Valdaitsev, A. Krasyuk, S. A. Nepijko, G. Schonhense, H. J. Elmers, I. Krug, and C. M. Schneider, Phys. Rev. B **76**, 134410 (2007).
[8] T. Devolder, C. Chappert, J. A. Katine, M. J. Carey, and K. Ito, Phys. Rev. B **75**, 064402 (2007).
[9] M. L. Schneider, M. R. Pufall, W. H. Rippard, and S. E. Russek, Appl. Phys. Lett. **90**, 092504 (2007).
[10] N. Biziere and C. Fermon, Appl. Phys. Lett. **92**, 092503 (2008).
[11] M. Bailleul, D. Olligs, and C. Fermon, Appl. Phys. Lett. **83**, 972 (2003).
[12] M. Bailleul, D. Olligs, and C. Fermon, Phys. Rev. Lett. **91**, 137204 (2003).
[13] C. Kittel, Phys. Rev. **71**, 270 (1947).
[14] R. Urban, G. Woltersdorf, and B. Heinrich, Phys. Rev. Lett. **87**, 217204 (2001).
[15] R. Arias and D. L. Mills, Phys. Rev. B **60**, 7395 (1999).
[16] L. Varga, A. Tanaka, K. Nagasaka, and R. Kondo, J. Appl. Phys. **85**, 5852 (1999).
[17] U. Ebels, *Spin Dynamics in Confined Magnetic Structures II*, edited by B. Hillebrands and K. Ounadjela (Springer, New York, 2003).
[18] T. Martin, M. Belmeguenai, M. Maier, K. Perzlmaier, and G. Bayreuther, J. Appl. Phys. **101**, 09C101 (2007).